A model for long-term climatic effects of impacts

T. Luder, W. Benz, and T. F. Stocker

Physics Institute, Space Research and Planetary Sciences, University of Bern, Bern, Switzerland

Received 25 February 2002; revised 23 April 2003; accepted 9 May 2003; published 16 July 2003.

[1] We simulated climatic changes following the impacts of asteroids of different sizes on the present surface of Earth. These changes are assumed to be due to the variations of the radiation energy budget as determined by the amount of dust globally distributed in the atmosphere following the impact. A dust evolution model is used to determine the dust particle size spectra as a function of time and atmospheric altitude. We simulate radiation transfer through the dust layer using a multiple scattering calculation scheme and couple the radiative fluxes to an ocean circulation model in order to determine climatic changes and deviations over 2000 years following the impact. Resulting drops in sea surface temperatures are of the order of several degrees at the equator and decrease toward the poles, which is deduced from the increasing importance of infrared insulation of the dust cover at high latitudes. While gravitational settling reduces the atmospheric amount of dust significantly within 6 months, temperature changes remain present for roughly 1 year irrespective of impactor size. Below 1000 m ocean depth, these changes are small, and we do not observe significant modifications in the structure of the ocean circulation pattern. For bodies smaller than 3 km in diameter, climatic effects increase with impactor size. Beyond this threshold, there is enough dust in the atmosphere to block almost completely solar radiation; thus additional dust does not enhance climatic deviations anymore. In fact, owing to interaction in the infrared, we even observe smaller effects by going from a 5 km impactor to larger diameters. *INDEX TERMS:* 0360 Atmospheric Composition and Structure: Transmission and scattering of radiation; 1630 Global Change: Impact phenomena; 4255 Oceanography: General: Numerical modeling; *KEYWORDS:* impact, Earth, dust, radiation, climate, atmosphere

Citation: Luder, T., W. Benz, and T. F. Stocker, A model for long-term climatic effects of impacts, *J. Geophys. Res.*, *108*(E7), 5074, doi:10.1029/2002JE001894, 2003.

1. Introduction

[2] Among the natural perils threatening living species, impacts of cosmic objects on Earth play an important role. However, since impact related hazards are relatively rare events by human measures, people generally do not bother about their consequences. Nevertheless, impacts have received widespread attention in the last few decades. They are recognized to be a crucial factor in the formation and evolution of the solar system. In addition, the impact of comet Shoemaker-Levy 9 on Jupiter in 1994 showed that collisions of celestial objects are not only features of the past. On Earth, geologists are searching for and investigating impact craters [*Grieve and Shoemaker*, 1994; *Ormö et al.*, 2001], the most prominent of which is the structure on the Yucatán peninsula, at the Cretaceous/Tertiary (K/T) boundary [*Hildebrand et al.*, 1991; *Pope et al.*, 1991; *Izett et al.*, 1991; *Sharpton et al.*, 1992; *Swisher et al.*, 1992].

[3] Using statistics of lunar craters, of near Earth asteroids, and of detections of explosions of meter-sized objects in the atmosphere, the frequency of asteroid impacts has been investigated [*Neukum and Ivanov*, 1994; *Chapman and Morrison*, 1994; *Morrison et al.*, 1994; *Brown et al.*, 2002]. It has been shown that the cumulative impact energy frequency distribution follows roughly a power law. Hits by meter sized objects occur on a weekly to monthly basis, while 50 m asteroids impact once every 1000 years, and 10 km or larger bodies approximately every 3×10^7 years [*Toon et al.*, 1997].

[4] An asteroid impact induces numerous consequences [*Toon et al.*, 1997]. Short-term effects include atmospheric and seismic shock waves leading to mechanical destruction on continental scales for a 10 km asteroid. Impacts into oceans initiate tsunami, which flood the coastal areas of the continents [*Hills et al.*, 1994; *Ward and Asphaug*, 2000]. In part, the land biomass catches fire owing to the heating of the atmosphere by the global reentry of high-speed impact ejecta [*Melosh et al.*, 1990; *Wolbach et al.*, 1990].

[5] Implications on longer timescales are the production of nitric oxide by the atmospheric shock waves [*Zahnle*, 1990], contamination by acid rain [*Lewis et al.*, 1982; *Prinn and Fegley*, 1987] and the partial destruction of the ozone layer. If the impact releases sulfur, sulfuric aerosols are reported to have a climatic effect like dust particles [*Kring et al.*, 1996; *Pope et al.*, 1997; *Pierazzo et al.*, 1998].

0148-0227/03/2002JE001894$09.00

[6] During the impact process, parts of the target and impactor are melted, vaporized or fractured. While fractured solid grains and boulders are lofted by the expanding gas plume, melted and vaporized material is ejected from the impact site at high velocity. At higher altitudes the gas condenses to small "dust" particles. These move on ballistic orbits around the globe and reenter the atmosphere from above to build up a global dust layer. It is usually assumed for a large enough projectile that this dust coverage can block sunlight preventing radiative energy to reach the surface. By reducing the surface solar energy flux and by changing the infrared radiation budget, impact produced dust clouds have implications for the climate. The same mechanism was considered in studies of the climatic response to nuclear wars [*Crutzen and Birks*, 1982; *Turco et al.*, 1983; *Schneider and Thompson*, 1988; *Robock*, 1989; *Turco et al.*, 1990, 1991].

[7] In order to derive the temperature drop induced over a marine and a continental surface, *Toon et al.* [1982] used a one-dimensional model of the atmosphere, in which dust particles from an impact by a roughly 20 km sized (diameter) asteroid were injected. They calculated that the surface continental air temperature would drop from a + 20°C preimpact value to −20°C. Temperatures started to drop below the freezing point 1.5 months after the impact and remained below 0°C another 6 months with the minimum being reached after 4 months. One year after the impact, the temperature deviation diminished from 40°C to 5°C. These strong land temperature variations contrast sharply with the temperature change over the ocean, for which the model by *Toon et al.* [1982] yielded −3°C. Over both land and ocean, the deviations were reversible.

[8] After the discovery of the K/T impact structure, *Sigurdsson et al.* [1992] noted that the target region was unusually rich in anhydrite, which should have yielded large quantities of sulfuric aerosols. Once deposited into the atmosphere, the influence of these aerosols on radiation and hence on climate is comparable to the dust induced darkness [*Pope et al.*, 1994; *Kring et al.*, 1996; *Pope et al.*, 1997; *Pierazzo et al.*, 1998].

[9] To make further progress in assessing the climatic effects of a dust layer following an impact, *Covey et al.* [1990, 1994] coupled a three-dimensional dynamic model of the global atmosphere with a simple parameterization of an evolving global dust layer and a dust radiation transfer code. They adopted an initial dust layer thickness corresponding to an asteroid diameter of 17 km, and let the amount of dust decline according a modified power law in time, obtained from an analytical fit to results from dust simulations given in the work of *Pollack et al.* [1983]. *Covey et al.* [1994] found air temperature changes of −39°C in central Africa, −33°C in southeast Asia, −39°C in Australia, and about −20°C in Eurasia, in Southern and Northern America.

[10] Those studies were restricted to a period of roughly 1 year following the impact, and they were focused on the atmospheric response. To reproduce surface temperatures, the atmospheric model by *Toon et al.* [1982] and *Pollack et al.* [1983] was thermodynamically coupled to a heat reservoir representing the terrestrial surface. The capacity of the reservoir was set to zero for continents, while for oceans, the surface heat capacity was set to a value corresponding to a mixed water layer 75 m deep. In the model by *Covey et al.* [1994], the ocean was represented by a 50–100 m deep heat reservoir.

[11] The total oceanic heat capacity is enormous. A global deviation in sea water temperature of 1 K corresponds to the irradiated solar energy integrated over approximately 1 year. This sharply contrasts with the heat capacity of the atmosphere. With respect to the ability to store thermal energy, the atmosphere corresponds to an oceanic layer with a thickness of only 3 m. To consider climate or surface temperature changes over periods longer than 1 year, it is therefore essential to take the oceans and their motion into account. First, over time, the atmosphere is brought by ocean convection in contact with water from originally deeper layers. Second and even more importantly, the oceanic circulation pattern may adapt to the disturbed energetic fluxes at the surface.

[12] To study these possible long-term effects of an impact, we use a model of the thermohaline ocean circulation. This climate model is integrated with boundary conditions corresponding to the radiative fluxes between the dust layer and the terrestrial surface. Such fluxes are calculated separately with a radiation transfer code.

[13] The radiative properties of the dust layer can be given in terms of its spectral transmissivity, reflectivity and the thermal emission, which are determined by the number density and the size distribution of the dust particles and the dust material. These quantities evolve owing to gravitational settling and coagulation of particles, making the optical properties of a dust layer time dependent. Since the residence time of dust grains in the atmosphere is a function of size, the main effect of coagulation is to reduce the lifetime of the dust layer. We do not focus our study to an impactor corresponding to the K/T event, but compare the climate response on the present-day Earth for impactor diameters ranging from 0.5 to 10 km.

[14] Most of the impact induced effects increase with the size of the impactor such as the magnitude of earthquakes, the amounts of gas and dust released, the area devastated by ignition of biomass, the extent of destruction of ozone layers, acidification, and the amplitude of tsunamis. However, while climatic changes measured by temperature changes also increase with size up to 3 km, they level off and even decrease slightly beyond the threshold of 5 km.

[15] Below, we first describe the overall structure and assumptions of the model, which consists of three modules. Then these modules are described in more detail with explanations of the physical background and the methods. Finally, we discuss various aspects of climatic change as a function of impacting asteroid size.

2. Structure of the Model

[16] For a better overview and portability of the code, we have split our model into three different modules, each handling separate aspects of the physical processes involved. These modules are (1) the time evolution of the dust injected in the atmosphere, (2) the radiation transport through the dust layer, and (3) the climate system.

[17] Starting with an equilibrium state of the climate, obtained by running the climate module without pertur-

bation for 10 kyr, we turn on the dust disturbance at $t = 0$. The one-dimensional dust evolution module is initialized with a dust density determined by the impactor diameter and particle size distribution along the vertical axis. Then gravitational settling and mutual coagulation of particles are followed, yielding a time- and height-dependent size distribution. For each of a set of predefined times, we use the second of the three modules to compute the corresponding solar and infrared radiation transport. Finally, the climate ocean module is used with boundary conditions given by the radiative fluxes calculated above.

[18] To allow for the interaction between radiation and the gaseous part of the atmosphere, we use transmissivities calculated with MODTRAN, a ''Moderate Resolution Transmittance'' Code, which is able to calculate atmospheric transmittance and radiance for frequencies from 0 to 1.5×10^{15} Hz at a resolution of 6×10^{10} Hz [*Kneizys et al.*, 1988; *Berk et al.*, 1989]. Each of the three modules is discussed in the following sections.

3. First Module: Dust Settling

3.1. Physics Included

[19] Our model does not take into account acid aerosols or global ignition of fires [*Wolbach et al.*, 1990], but focuses on dust from the ejecta. The amplitude of the climate response to an impact depends on the thickness and the persistence of the dust layer in the atmosphere, determined by the evolution of the particle density and size distribution. These quantities are computed by the first module.

[20] After a dust particle is injected into the top of the atmosphere, its vertical velocity is determined by gravitational settling and Brownian motion. Once it crosses the tropopause, it is quickly removed from the atmosphere by rainout, making the tropospheric residence time short in comparison to the time the particle has spent above the tropopause. Therefore we neglect the lifetime of the dust particles in the troposphere.

[21] Numerical calculations [*Argyle*, 1988; *Durda et al.*, 1997] of the K/T ejecta trajectories do not show a pure spherically symmetric distribution of dust particles around Earth. However, except for a peak in the vicinity of the impact location and at the antipode, the spread in ejecta thickness is within a factor of two of the mean thickness [*Argyle*, 1988]. It is known from volcanic eruptions, which act as a point source of stratospheric aerosols, that dust and soot particles in the stratosphere are quickly redistributed in zonal bands. Therefore the initial inhomogeneities of the distribution are smeared rapidly on a global scale. We assume that the worldwide distribution of particles is geographically homogeneous. As a consequence, our model is not specific to the location of the impact.

3.1.1. Settling Speed

[22] The settling speed w of a dust particle is given by the equilibrium between the gravitational force and the gas drag, which for laminar gas flow is given by the Stokes drag equation. However, at atmospheric levels above the troposphere, the condition of laminarity is violated for typical micron-sized particles. If the particle radius is smaller than the mean free path λ_g of the gas, the Stokes drag has to be modified by the Cunningham correction factor C. C depends on particle radius r and atmospheric conditions at altitude z. This results in

$$w(r,z) = \frac{2}{9} \cdot \frac{r^2 \rho g C(r,z)}{\eta(z)} \tag{1}$$

for the settling velocity. In this approach, the local viscosity $\eta(z)$ and mean free path are determined according to *Otto et al.* [1999] and *Park et al.* [1999].

3.1.2. Sticking of Particles

[23] Collisions between dust particles occur owing to Brownian motion and differences in settling speeds (equation 1) between particles of different sizes. However, there are arguments [*Toon et al.*, 1982] that different settling speeds of particles do not lead to mutual collision. This viewpoint rests on the observation that particles suspended in the air would flow around each other rather than collide. Therefore *Toon et al.* [1982] only used Brownian motion as a driver for collisions in their calculations.

[24] We follow the argument by *Toon et al.* [1982], but allow for coagulation due to settling in the free molecular regime: if the atmospheric mean free path, which increases with height, exceeds the size of particles, then in our model dust grains do collide owing to differences in settling speed. Coagulation due to Brownian motion is always allowed for. To check the influence of coagulation induced by settling, we compare (sections 3.3 and 6) the results of calculations in which collisions owing to relative settling are (1) fully included or (2) restricted to the nonlaminar flow regime to model runs where coagulation is totally excluded (3).

[25] Once two particles collide, there is a probability for them to stick together and give rise to a larger grain. Therefore the particle size spectrum is a function of time. Sticking of two spherical particles occurs if the kinetic energy of the system is lower than a critical value E_{cr} [*Chokshi et al.*, 1993; *Dominik and Tielens*, 1997]. Experimental studies by *Poppe et al.* [2000] have confirmed this behavior of the sticking probability. However, they have found larger values for the critical velocities than is predicted by the findings by *Dominik and Tielens* [1997]. Since in our study, the critical velocity has to be determined for a wide range of parameters not being covered by experimental results, we apply the theoretical expressions.

3.1.3. Advection-Coagulation Equation

[26] For mathematical reasons, it is reasonable to study the evolution of the dust distribution by expressing the number density not as a function of particle radius r but particle volume v. (Volumes of sticking particles can be added, while handling radii would need unnecessary expensive calculations.)

[27] The advection-coagulation equation is then given by

$$\begin{aligned}\frac{\partial n(v,z,t)}{\partial t} = & -\frac{\partial (w(v,z)\cdot n(v,z,t))}{\partial z} \\ & - n(v,z,t)\int_0^\infty \beta(v,\bar{v},t)\cdot, n(\bar{v},z,t)d\bar{v} \\ & + \frac{1}{2}\int_0^v \beta(v-\bar{v},\bar{v},\ z)\cdot n(v-\bar{v},z,t)\cdot n(\bar{v},z,t)d\bar{v},\end{aligned} \tag{2}$$

where $w(v, z)$ are the local settling velocities, and $n(v, z, t) \cdot dV \cdot dv$ is defined as the number of particles with a particle volume in the interval $[v, v + dv]$ and in the atmospheric

volume dV at height z and time t. Note that v refers to particle volume, while w denotes settling velocity. The first contribution on the right hand side of equation (2) is the advection term imposed by gravitational settling. The second and the third term are the sink and the source contribution owing to particle coagulation. β is the coagulation kernel. The kernels due to Brownian motion and due to settling speed are given by

$$\beta_{Brown} = \frac{2kT(z)}{3\eta(z)} \cdot \left(v_1^{1/3} + v_2^{1/3}\right) \cdot \left(C(v_1,z)v_1^{1/3} + C(v_2,z)v_2^{1/3}\right) \tag{3}$$

and [*Warneck*, 1988, p. 288]

$$\beta_{Setting} = \pi\left(v_1^{1/3} + v_2^{1/3}\right)^2 \cdot |w(v_1,z) - w(v_2,z)|. \tag{4}$$

3.1.4. Initial Dust Distribution

[28] As noted above, we assume that the initial amount of dust and the initial size distribution of the grains do not depend on the geographical location. At $t = 0$, the dust particles are homogeneously distributed throughout the atmosphere in a layer between $z = 20$ km and $z = 100$ km. The limits chosen do not much affect the climatic response. At the upper boundary, the settling speeds of micron-sized particles are several tens of meters per second, and therefore they fall several kilometers within minutes. These changes are too rapid to have any influence on the climate. Intuitively, since the settling velocities at 20 km are much smaller (order of meters/hour), it would seem that the choice of the lower boundary could be quite important. However, in their investigation of the evolution of an impact dust cloud, *Toon et al.* [1982] injected the dust first between 12 km and 42 km, and then between 66 km and 88 km. They found that the optical depth of the evolving dust layer is only slightly sensitive to the initial height of the dust. *Covey et al.* [1990] started with a dust layer between about 15 and 30 km. Since it is improbable that a dust grain can be found in the lowest parts of the stratosphere shortly after its penetration in the upper atmosphere, we choose the lower boundary somewhat higher, 20 km.

[29] Indeed, the exact choice of the lower boundary is not relevant for the climatic effect. Figure 1 shows that the time at which the lowest dust particles reach the tropopause is almost independent of the choice of the initial lower boundary for values between 20 and 30 km altitude. This behavior is explained by the dependence of the settling speed on altitude. Since the speed of higher particles is larger than the speed of particles at lower altitudes, the initial differences in the position of the lower boundary decrease. Hence between 2 and 3 months after the impact, the penetration of the dust into the troposphere occurs concurrently for dust clouds starting at different altitudes.

[30] The initial particle size spectrum cannot be determined from past impacts by looking at the sedimentary record since weathering and compaction have blurred the size distribution of deposited particles. However, we can use volcanic ejecta to specify an initial size distribution. *Farlow et al.* [1981] determined radii of aerosols which were collected in the stratosphere between and after the eruptions of Mount St. Helens. They fitted the results with a lognormal

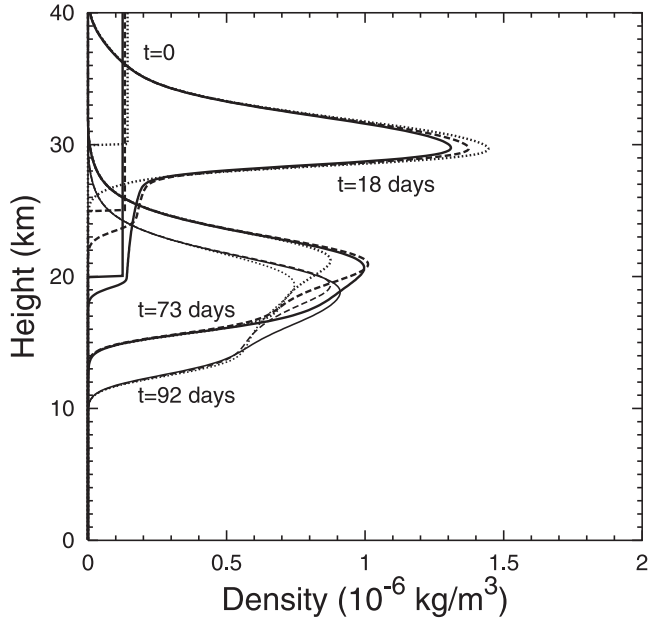

Figure 1. Evolution of the particle density profile for three initial vertical distributions (solid: 20 to 100 km, dashed: 25 to 100 km, and dotted: 30 to 100 km). In all cases, the initial column density is 0.01 kg/m^2, corresponding to an impactor with a diameter of 2.2 km. Since settling speed increases approximately exponentially with altitude, the front starting at 30 km height propagates faster than the particles initially at 20 km height. Therefore the vertical positions of these particles converge with time. Owing to this effect, the lower dust boundaries of the three cases reach the troposphere approximately simultaneously. The high densities in the upper part of the dust cloud result from the accumulation of fast-falling particles from higher altitudes.

distribution and found modal radii from 0.48 μm to 0.94 μm. *Jaenike* [1988] investigated stratospheric aerosols 1 year after volcanic eruptions and gives a lognormal size distribution with a modal radius of about 0.217 μm. This smaller value is explained by the fact that after 1 year larger particles have had time to move out of the atmosphere, thus shifting the size distribution toward smaller values.

[31] *Toon et al.* [1982] used a lognormal distribution with modal radius of 0.5 μm for the initial particle size distribution in their simulations. In sensitivity tests they found only a small dependence of the cloud's evolution on the initial size spectrum. This is consistent with our own results that the evolution of the amount of particles in a dust layer is insensitive to the initial modal radius in the range from 0.5 μm to 0.9 μm. Therefore we adopt an initial size spectrum given by a lognormal distribution

$$\frac{1}{\sqrt{2\pi}r\ln\sigma} \cdot \exp\left(-\frac{\ln^2(r/r_0)}{2\ln^2\sigma}\right) \tag{5}$$

with modal radius $r_0 = 0.7$ μm and dispersion parameter $\sigma = 1.25$. Since particles larger than a few microns have large fall speeds and quickly drop out of the atmosphere, rendering them irrelevant for climatic changes, we truncate the particle size distribution at 4 μm diameter and neglect larger sizes.

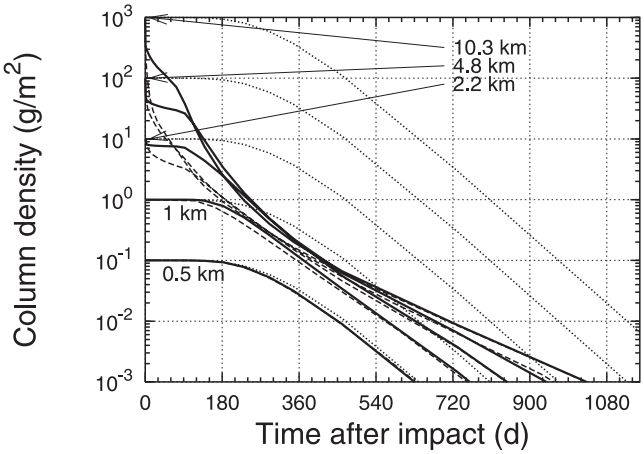

Figure 2. Evolution of column density of micron-sized dust particles above the tropopause (fixed at 13 km height) for five impactor diameters (0.5, 1, 2.2, 4.8, and 10.3 km; see equation (6)). Coagulation of dust particles occurs owing to both Brownian motion and gravitational settling (dashed lines), owing to both Brownian motion and settling, but restricted to the free molecular flow regime (solid lines), while dotted lines show the dust evolution when coagulation is completely ignored.

[32] Estimates of the amount of the dust being injected into the atmosphere and globally distributed are reviewed by *Toon et al.* [1997]. It is found that the mass in submicron-sized particles constitutes only a small fraction of the total ejecta, roughly 30% of the impactor's mass. With this assumption, the worldwide dust column density is

$$L = \frac{0.3\rho d^3}{24R_E^2}, \tag{6}$$

where ρ, d, and R_E are the mass density and the diameter of the bolide, and the radius of Earth. In the equation above, we have used a surface area of the planet of $4\pi R_E^2$ and a mass of $\pi\rho d^3/6$ for the impactor. Assuming $\rho = 3000$ kg/m^3, we find L = 0.0001, 0.001, 0.01, 0.1, and 1 kg/m^2 for bolides with diameter d = 0.5, 1, 2.2, 4.8, and 10.3 km.

3.2. Implementation of the Dust Module

[33] The dust evolution module simulates the temporal, one-dimensional behavior of the dust distribution in the atmosphere above the tropopause, which is governed by the advection-coagulation equation (2). The dust-size distribution is represented by 100 logarithmically distributed particle volume bins representing radii from 0.2 μm to 2 μm. The vertical axis is subdivided into 1000 uniform levels from 0 km to 100 km height; particles are neglected once they cross the tropopause. We solve equation (2) using a first-order explicit upwind scheme. The advection part is solved with a flux based method, and the coagulation integrals are transformed into sums over the size bins.

3.3. Results From the Dust Evolution Model

[34] The model indicates that the dust persists above the tropopause for about half a year. Figure 2 shows the evolution of the column density of dust for five initial amounts (10^{-4}, 0.001, 0.01, 0.1, 1 kg/m^2). In the standard case, settling coagulation is only included in the free molecular flow (see section 3.1.2). High initial dust amounts (0.1 and 1 kg/m^2) thin out within days, while lower amounts show a slower evolution. This difference in behavior is explained by the quadratic dependence on number density of the coagulation rate, which leads to larger particles for higher densities, and hence to higher settling speeds.

[35] If the settling coagulation is not restricted to the free molecular flow but is also allowed for in the continuum flow, the dust column densities drop not only during days but for months in the 0.01, 0.1, and 1 kg/m^2 scenarios. After 3 months, a dust density of 0.001 kg/m^2 is reached. In the cases with low initial amounts of dust (10^{-4} and 0.001 kg/m^2), the difference from the standard case is marginal.

[36] Figure 2 also shows the evolution of the column density for the case of no coagulation. Under this unrealistic assumption, it takes 450 days to decrease the number of dust particles by a factor of 10, which is much longer than in the standard case. Therefore coagulation is a significant factor for the lifetime of a dust layer.

[37] Figure 3 shows the profile of the dust mass density for the five impactors (0.5, 1, 2.2, 4.8, 10.3 km in diameter) 1.5, 4.5, and 12 months after the impact. For larger initial amounts of dust, the peak density for a given time is located at a lower altitude than for lower amounts of dust. This reflects again the importance of coagulation and the size dependence of the settling speed.

4. Second Module: Radiation Transfer Through a Dust Layer

4.1. Introduction

[38] The calculation of Earth's surface radiation budget involves quantifying both the spectral radiation transfer through the dust layer and the thermal emission of the dust

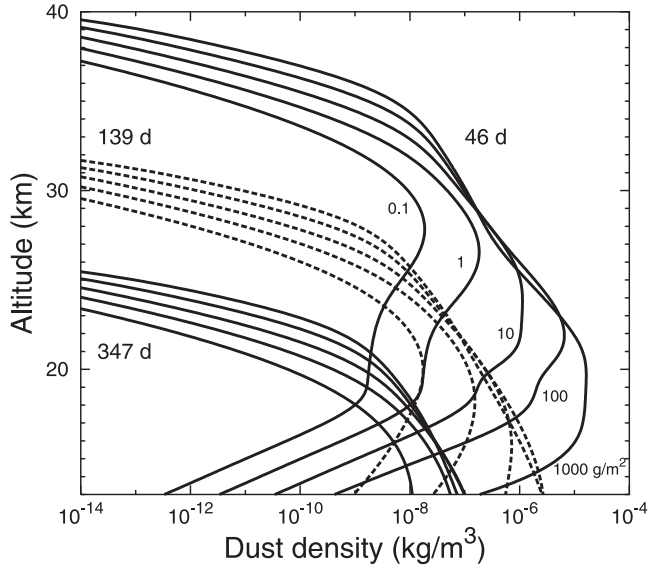

Figure 3. Dust density profiles at 3 times for 5 initial dust column densities (10^{-4}, 0.001, 0.01, 0.1, and 1 kg/m^2). If equation (6) is applied, these values correspond to impactor diameters of 0.5, 1, 2.2, 4.8, and 10.3 km. Particles below 13 km are not considered because they are removed from the atmosphere by rainout.

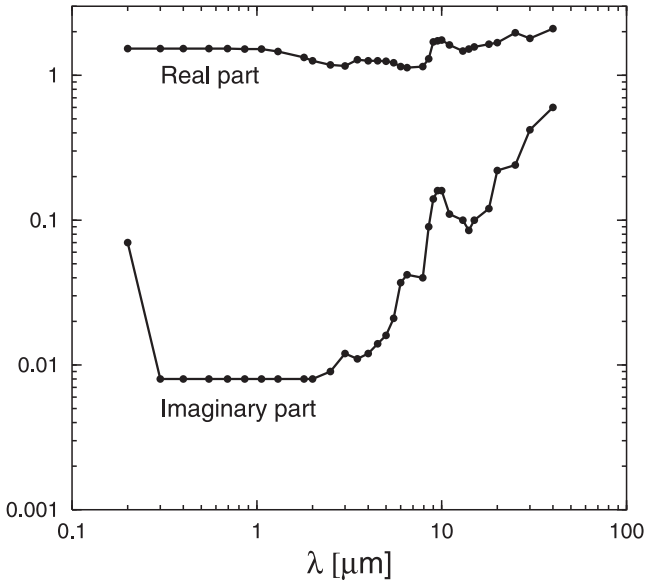

Figure 4. Real and imaginary part of the spectral complex indices of refraction [*Jaenike*, 1988].

particles and the terrestrial surface. Since the dust grains are not only absorbers but also scatterers of radiation, the intensity of solar radiation does not simply decay exponentially with the penetration depth. In general, a photon may be scattered several times, thus multiple scattering contributes significantly to the radiation field. Because radiation that is scattered several times has lost its initial direction, the total radiation field is diffuse. Whether multiple scattering is important in an optically thick medium is determined by the ratio of scattering and absorption cross section. These quantities are given by the process of single scattering, therefore the understanding of the single scattering is essential to treat multiple scattering. Single scattering quantities are calculated by means of Mie theory.

[39] Since the optical properties of a dust layer depend on the ratio between particle size and wavelength as well as the complex index of refraction (Figure 4), which itself is a function of wavelength [*Jaenike*, 1988] radiation transfer calculations have to be performed for a number of different wavelengths distributed over the spectrum. We selected 63 discrete, exponentially distributed wavelengths λ_i in the range from 0.25 μm to 80 μm.

[40] To solve the radiation transfer equations in a scattering and absorbing medium, a number of numerical techniques are available. Many are discussed by *Hansen and Travis* [1974], *Irvine* [1975], *Liou and Sasamori* [1975], *Stamnes* [1986], *Goody and Yung* [1995], and *Thomas and Stamnes* [1999]. We adopted the doubling-adding method because (1) it is considered as accurate, (2) results obtained during the iteration process have a physical meaning, and (3) it allows a straight forward implementation of the intrinsic emission of thermal radiation within the dust layer.

[41] The original form of the doubling and adding method calculates transmission and reflection properties of a dust layer. Here we apply the doubling and adding concept to determine solar and infrared fluxes not only at the boundaries of the cloud, but also within the layer. The concept consists of using known transmission and reflection properties of two adjacent layers to calculate reflection and transmission of the combined one. If the properties of the two layers are not identical, they are "added" while two identical layers are "doubled." By construction, the application of the method is restricted to plane parallel geometries. The key idea of the method is to use very optically thin adjacent slices ($\tau \ll 1$) for which optical characteristics can be computed from single scattering theory [*Goody and Yung*, 1995, p. 346] and to "double" these slices until the desired optical depth is reached. Since the optical depth increases exponentially with the number of iteration steps, a substantial thickness is obtained very quickly. In general, the whole dust layer does not have a vertically homogeneous structure; therefore its radiative attributes cannot be acquired directly with the doubling procedure. The dust layer has to be subdivided into a number n of sublayers L_i ($i \in \{1, \ldots, n\}$, with $i = 1$ for the topmost sublayer and $i = n$ for the lowest one) characterized by different temperatures, dust size distributions, and number densities. Within each sublayer, it is assumed that these properties are constant. Thereby the optical characteristics of each can be obtained using the doubling method above.

[42] The lower boundary condition is determined by the surface of Earth, which absorbs, scatters and emits radiation. These properties of the terrestrial surface are represented by an additional sublayer L_{n+1}.

[43] For a given solar position and infrared input from below, the dust temperature profile in the layer is calculated assuming that every sublayer is in local radiative equilibrium. Hence the sum of input and output energy fluxes at the lower and upper boundary of each sublayer has to vanish.

[44] In dust layers with small or moderate optical thickness, the solar radiation is absorbed throughout the layer, which leads to a relative smooth temperature profile. However, in optically thick layers, where most of the solar energy is absorbed in the uppermost region, the temperature shows a sharp increase in the uppermost region of the layer. To resolve this temperature structure, the geometrical thickness of the sublayers in this zone must be small, while in lower parts where the temperature profile is smooth, a lower resolution is quite adequate. We achieve the appropriate results by choosing sublayers in such a way that their optical thickness increase exponentially from the top to the bottom of the cloud.

4.2. Test of the Radiation Transfer Code

[45] In order to test our implementation of the doubling and adding method, we compared radiation transfer results to independent Monte Carlo calculations. In the Monte Carlo code, photons are sent stochastically through the dust cloud until they are absorbed or leave the cloud at the upper or lower boundaries. The fraction of traversing photons is equal to the transmission, while the fraction of photons leaving at the upper cloud boundary yields the cloud's reflectivity.

[46] In the first test with monochromatic photons, we compare the transmission coefficient through a homogeneous dust layer, assuming isotropic scattering. The results are shown in Figure 5 for a range of dust cloud parameters such as total optical depth and single scattering albedo. We find a good agreement between the two independent methods. For single scattering albedos between 0 and 0.5, the transmissions do not vary much. However, a higher single

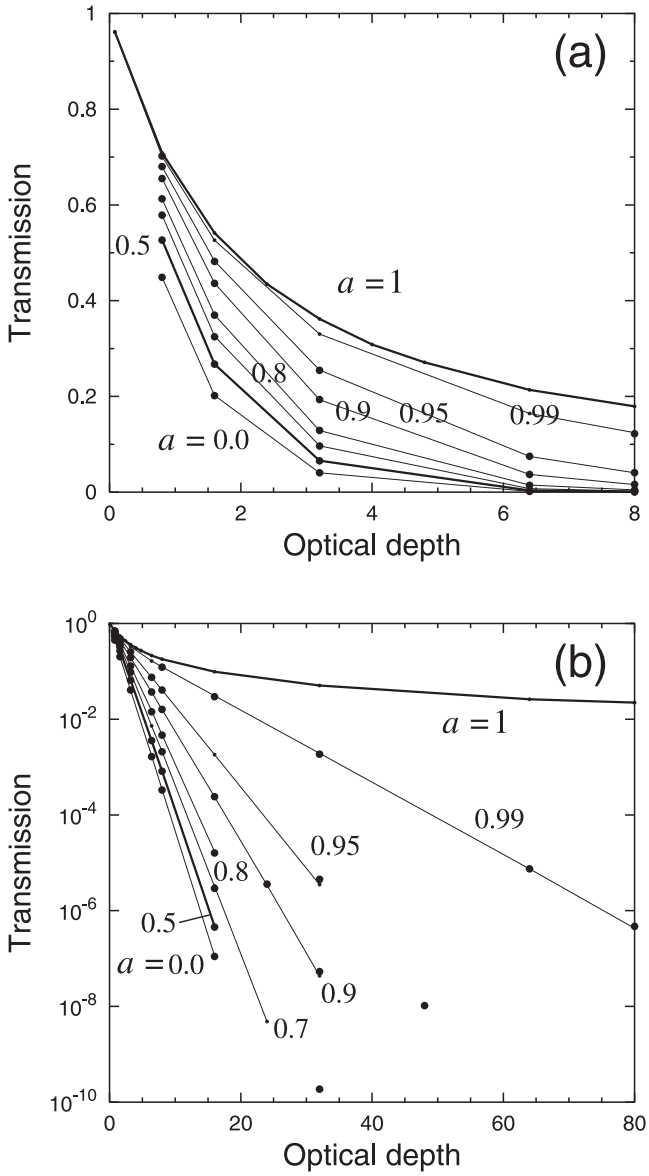

Figure 5. Transmission of a dust cloud as function of optical depth for several single scattering albedos *s* ranging from 0 to 1. The straight lines are calculated with a Monte Carlo method. Points represent results from the doubling and adding code. Figures 5a and 5b show the same data with different axis scale.

scattering albedo leads to a significant increase of the transmission, which is good evidence for the importance of the scattered, diffuse radiation.

[47] The second test (Figure 6) considers reflection and transmission of a given dust cloud for a range of wavelengths. Again there is good agreement between the Monte Carlo method and the doubling and adding technique, making us believe that our doubling and adding code is adequate.

[48] The transmission shows a large variability with wavelength. While at the maximum of the solar spectra at 0.55 μm, the transmission is below the resolution of Figure 6, the transmission of infrared radiation is higher by several orders of magnitude. Since a substantial part of solar energy is contained in the near infrared spectrum (more than 30% in wavelengths larger than 1 μm), the cloud transmits much more solar energy integrated over the solar spectrum than could be estimated from transmission measurements at wavelengths in the visible.

4.3. Characteristics of Obtained Energy Fluxes and Optical Depths

[49] Figure 7 shows the net flux of solar and infrared radiative energy at the surface below a dust layer as a function of the amount of dust, neglecting the gaseous part of the atmosphere. Four solar zenith angels (A: 4°, B: 36°, C: 64°, D: night side) are considered. For low dust column densities (e.g., 10^{-6} kg/m^2), the net input flux converges to $(1-a)S_0\cos(\theta) - \varepsilon\sigma T^4$, where a, ε, T, S_0, θ, and σ are surface albedo, emissivity and temperature, solar constant, solar angle measured from the zenith and Stefan-Boltzmann constant, respectively. For high solar position cases (4°, case A; and 36°, case B), the net input energy decreases as expected with increasing amount of dust. However, as the Sun nears the horizon (64°, case C), this monotonic trend no longer holds true as the total flux becomes dominated by infrared radiation. The resulting net flux can best be understood by considering the night side case (>4°, D), where there is no solar energy input at all. For small dust column densities, the radiation field consists only of terrestrial surface emission ($\varepsilon\sigma T^4$). However, with increasing amounts of dust, more terrestrial radiation is absorbed by the dust and re-radiated in the infrared, partly back to Earth, which explains the reduction in the net energy loss of the surface. (This is also why clear nights are colder than cloudy ones.) The effect increases with the amount of dust until all terrestrial radiation

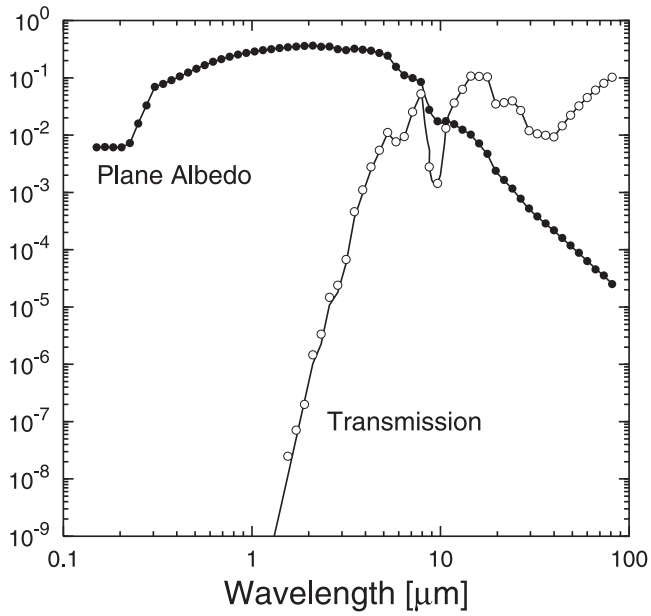

Figure 6. Spectral reflection and transmission of a dust layer for 63 wavelengths. The column dust density is 0.1 kg/m^2 with a particle density of 3000 kg/m^3. The particle size distribution is lognormal with modal radius 0.7 μm and dispersion parameter σ = 1.25. Complex indices of refraction are given in Figure 4. The solid line represents results from the doubling and adding technique; circles indicate the numbers from the Monte Carlo method.

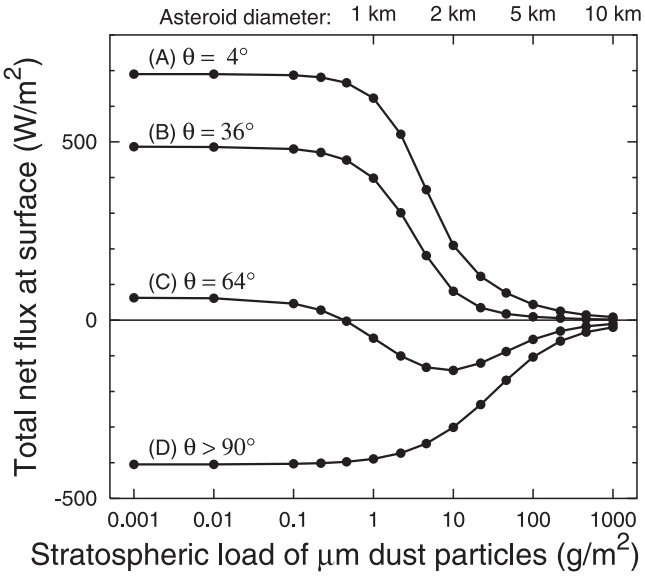

Figure 7. Net radiation energy at Earth's surface as a function of dust column density. The position of the Sun is 4, 36, and 64 degrees below zenith, and below the horizon ($\theta > 90°$), respectively. The given surface temperature, infrared emissivity and albedo for visible light are 295 K, 0.95, and 0.2.

is absorbed by the dust layer. In very thick clouds, this infrared absorption and re-emission is restricted to the lower region of the dust layer, establishing a radiative equilibrium between Earth and this region, and decoupling the terrestrial radiation from space. Therefore the net flux at the surface converges to zero.

[50] This insulating behavior of a cloud of dust also explains why even for high solar positions (Figure 7, (cases A and B)) the net flux converges to zero with increasing dust column densities. An optically thick cloud decouples the terrestrial surface from the solar input energy by scattering the solar radiation back, while loss of infrared energy is prevented. We conclude that high amounts of dust act as a barrier against both visible and infrared radiation.

[51] Figure 7 shows an interesting feature for intermediate amounts of dust. In the low solar position case (C) the net surface flux decreases from 10^{-4} kg/m^2 for increasing amounts of dust, reaching a minimum at 0.01 kg/m^2. For higher amounts of dust, it starts increasing until it eventually approaches zero. The reason for this minimum is that the reduction of the solar energy at the surface is substantial already for low dust levels, while the infrared insulating effect only becomes important for amounts of dust above 0.010 kg/m^2.

[52] The minimum can only exist, if the solar and infrared fluxes are approximately equal, as in case (C). Both cases with high solar position (A and B) do not show this behavior. In the unperturbed situation (amount of dust = 0) of case (A), solar heating is three times the terrestrial infrared loss. This predominance of solar energy remains even for increasing amounts of dust, preventing the existence of a minimum.

[53] Owing to dust settling, the opacity of the cloud decreases with time. Figure 8 shows the evolution of the optical depth at 0.56 (solid line) and 7.87 μm (dotted) wavelength after impacts of bolides 0.5, 1, 2.2, and 4.8 km in diameter. As indicated by Figure 6, the optical thickness of a dust layer in the infrared is only a small fraction of the thickness in the visible, which is important for the frequency spectrum below the layer. The significant but slow change in optical depths in the first 3 months following the impact originates from shifts in size distribution. Only after 3 months the lower front of the dust layer reaches the troposphere, quickly reducing the stratospheric amount of dust. Dust below the stratosphere is not considered; hence optical depths drop sharply about 100 days after the impact.

[54] Figure 9 represents the evolution of transmission in the visible ($\lambda = 0.55$ μm). Owing to high initial coagulation rates, the optical thickness of the cloud decays, and transmission strongly increases in the first few days. For the larger dust loads, the recovery of transmission slows down but accelerates again after roughly 100 days, when the lower edge of the cloud reaches the troposphere (see also Figure 8). This characteristic time depends on the initial amount of dust, but only marginally on the initial altitude of the cloud (section 3.1.4).

[55] For the 10 km and 5 km impactor scenarios, the initial darkness is strong enough to stop photosynthesis, according to the threshold (1% of normal light level) assumed by *Toon et al.* [1982]. Our transmissions do not perfectly match that of *Toon et al.* [1982, Figure 8], mainly because we use slightly different complex indices of refraction.

4.4. Radiation Spectrum Below the Dust Layer

[56] While impact induced climate changes depend on the integrated spectral energy fluxes, there are biological processes such as visual sight and photosynthesis, which depend on the transmission in the visible window of the radiation spectrum. In Figure 10 we plot the spectrum of

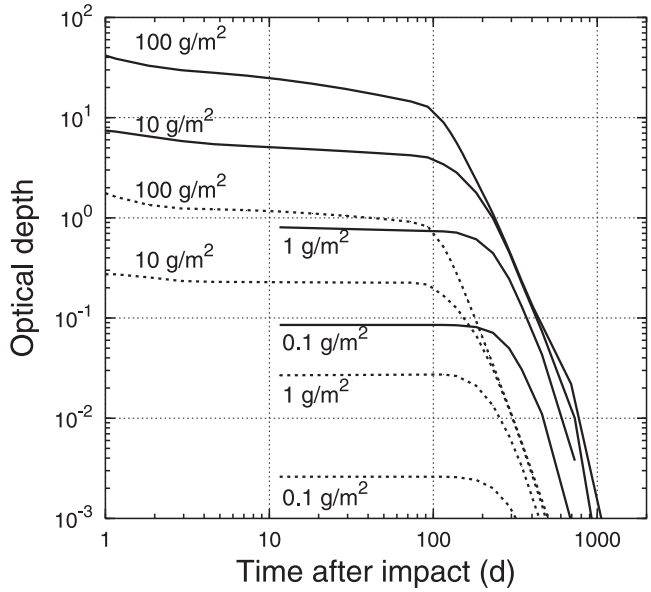

Figure 8. Evolution of optical depth at 0.56 μm (solid lines) and at 7.87 μm (broken lines) for four initial dust column densities (10^{-4}, 0.001, 0.01, and 0.1 kg/m^2). Compare to *Toon et al.* [1982, Figure 6].

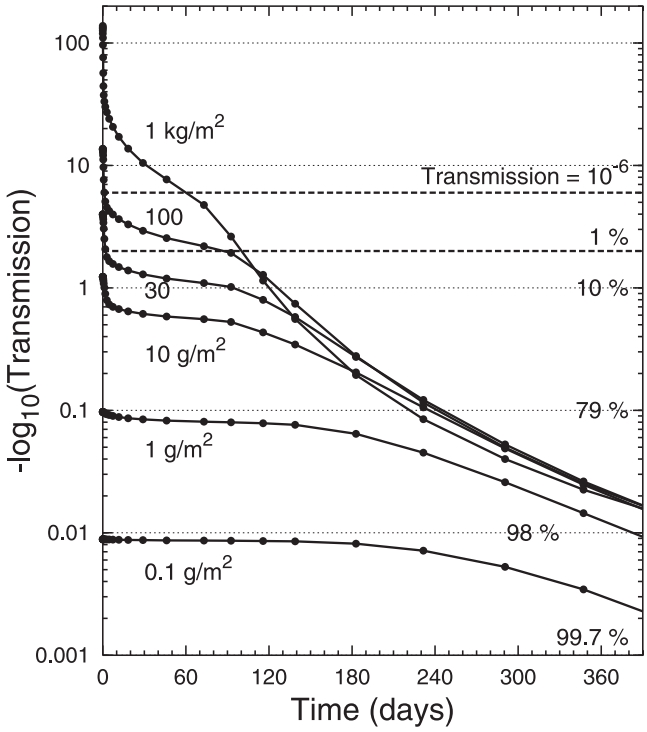

Figure 9. Evolution of transmission at λ = 0.55 μm through dust clouds with initial column densities of 10^{-4}, 0.001, 0.01, 0.03, 0.1, and 1 kg/m^2. Using equation (6), these amounts correspond to diameters of impacting asteroids of 0.5, 1, 2.2, 3, 4.8, and 10.3 km (solid lines). The dashed lines indicate the light level of full moonlight and a conservative estimate for the threshold of photosynthesis given by *Toon et al.* [1982]. Note that transmission may depend strongly on wavelength (Figure 6); therefore λ = 0.55 μm is not representative for the transmission of the total solar energy. Since the rate of coagulation increases with particle number density, the 1 kg/m^2 cloud soon consist of larger particles than those in the 0.1 kg/m^2 cloud. These high coagulation rates, leading to larger particles, increase the settling speed. Hence the transmission increases faster in the case of a 1 kg/m^2 scenario than for the clouds with smaller initial column densities.

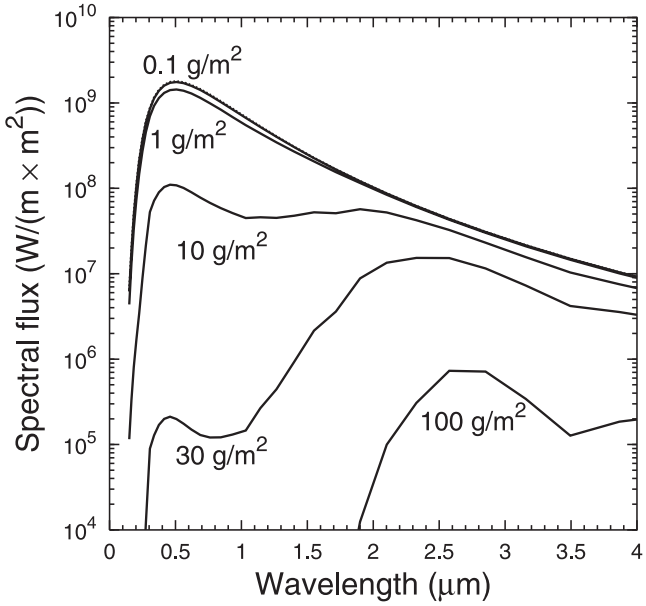

Figure 10. Spectral solar flux below dust layers with 10^{-4}, 0.001, 0.01, 0.03, and 0.1 kg/m^2 thickness (corresponding impactors diameters are 0.5, 1, 2.2, and 4.8 km, given by equation (6)). In the 10^{-4} kg/m^2 case, the deviation from a normal solar spectrum is hardly visible on the scale of this diagram.

solar radiation as emerging below the initial dust layer. This figure dramatically shows the much stronger damping of radiation in the visible than in the infrared. Therefore a dust cloud threatens those systems limited to optical wavelengths (e.g., the biosphere) much more than others which depend in first approximation only on total energy fluxes (e.g., climatic processes). The strong dependence of dust layer opacity on wavelength is also highlighted in Figure 11, which shows the spectral transmission of dust layers for wavelengths between 0.15 and 83 μm. Transmission is defined here by the ratio of the spectral fluxes at the bottom and at the top of the dust layer.

5. Third Module: Thermohaline Ocean Circulation

[57] To investigate the long-term climatic effects, we use a two dimensional, zonally averaged dynamic ocean circulation model [*Wright and Stocker*, 1992; *Stocker et al.*, 1992]. It represents the Atlantic, Indian, and Pacific basins in their present-day shape, connected with the Southern Ocean. A simple thermodynamic sea ice model is included.

[58] The oceanic spatial grid consists of 14 vertical and 9 to 14 horizontal cells, depending on the basin, with a

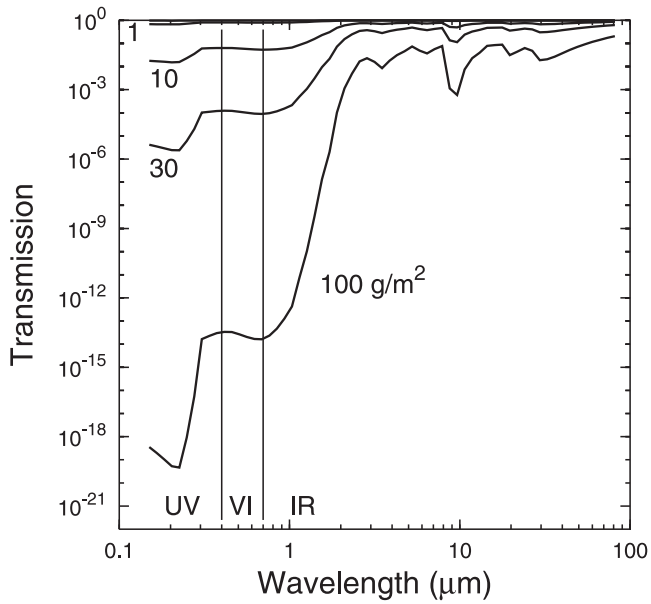

Figure 11. Spectral transmission between 0.15 and 83 μm through dust layers with 0.001, 0.01, 0.03, and 0.1 kg/m^2 column density. Vertical lines at 0.4 and 0.7 μm indicate the boundaries between the UV, the visible and the IR regime [*Thomas and Stamnes*, 1999].

meridional width of between 7.5° to 15°. In this model, the governing equations are written in spherical coordinates and include hydrostatic, Boussinesq and rigid-lid approximations. Momentum equations are balances between Coriolis forces, horizontal pressure gradients and zonal wind stress. Time dependence enters via the equations for temperature and salinity, including vertical and meridional advection, diffusion and convection. Horizontal and vertical eddy diffusivities are taken as constant (1000 m^2/s and 4×10^{-5} m^2/s, respectively).

[59] With present-day conditions this model shows the deep water formation in the northern Atlantic and in the Southern Oceans, and upwelling of waters toward the surface in the Pacific and the Indian Oceans. Observed temperature and salinity patterns as well as meridional fluxes of heat and freshwater are well reproduced.

[60] The atmospheric part is based on the balance of energy and does not contain a circulation model. Fluxes of energy and water within the atmosphere, between ocean and air, and between continents and oceans are parameterized in terms of surface air temperature. The model does not take into account climatic processes on land such as snow.

[61] Before the dust injection, the model oceans are in a steady state that represents the present climatic situation. At $t = 0$ the given dust load is injected as described in section 2, and the climate evolution is followed together with the changes in the dust cloud. After the column density of dust has fallen below the 10^{-6} kg/m^2 level, we let the climate model run with preimpact boundary conditions until the integration time reaches 2000 years.

6. Results and Parameter Studies

[62] In this section, focusing on climatic change, we present temperature variations after the impacts of asteroids with 0.5, 1, 2.2, 4.8, and 10.3 km in diameter. These results are followed by parameter sensitivity studies in order to underline the stability of the model. The parameters being changed are the imaginary index of refraction in the Mie calculations and the vertical eddy diffusivity for temperature and salinity in the ocean model. Then we have checked the effects of an artificial one week cessation of the dust evolution immediately after the ejecta is globally distributed. This accounts for uncertainties in the process of worldwide injection of dust into the atmosphere. Another test consists of running the dust evolution slower by a factor of 10. Finally we consider the implications of modified dust coagulation.

[63] The assumption that the impact generated dust is distributed worldwide imposes a lower limit on the asteroid diameter. Impacts of 1 km sized objects are believed to have enough energy to distribute dust particles on a global scale by ballistic transport, while impacts of smaller asteroids contaminate only the regional atmosphere [*Melosh*, 1989, Figure 11.6]. Hence although dust is then redistributed by atmospheric winds, the main effects of small impacts are probably local instead of global. However, to be conservative, the smallest asteroid diameter treated in this study is 0.5 km. For objects of this size, the mean recurrence time of impacts on Earth amounts to 3×10^4 years [*Toon et al.*, 1997]. The largest impactor considered is 10 km in diameter, corresponding to roughly 3×10^7 years between impacts on the average. Note that in the early study by *Toon et al.* [1982] the initial column density of micron-sized particles was 10 kg/m^2. This amount corresponds to an impactor 22 km in diameter (equation 6).

6.1. Temperature Changes Following Impacts

[64] Owing to the dust immersion in the atmosphere, surface temperatures generally decrease globally after the impact. Sea surface temperature (SST) deviations from preimpact values show three prominent features: 1. Negative deviations are most pronounced at the equator and decrease with latitude (Figure 12). 2. If the initial dust column density exceeds roughly 0.03 kg/m^2 (which corresponds to a 3 km sized asteroid), high-latitude temperatures show positive excursions (Figure 12). 3. The temperature response at low latitudes does not increase monotonically with asteroid size (Figure 13). This means that there is an optimal asteroid diameter in the sense of equatorial temperature drop.

[65] To understand these results, it is important to take into account both the solar and the terrestrial thermal radiation flux. A dust layer reduces these fluxes, however, not uniformly over the wavelength spectrum, as was shown in Figure 11. In the visible, the transmission of a layer is much smaller than in the infrared. Since for thermal energy or for temperature at Earth's surface, solar radiation is a source and terrestrial infrared emission is a sink, a dust layer has qualitatively different effects depending on the amount of dust. A very thin layer interacts only slightly with solar radiation and has even a smaller effect in the infrared, therefore the terrestrial temperature will not react strongly. A dust layer of intermediate density blocks sunlight significantly, while in the infrared, it can be still virtually transparent. Under this condition, Earth's surface temperature will decline. However, a thick layer is opaque not only in the visible but also in the infrared. Compared to the intermediate layer, the already reduced solar flux does not change much, but owing to absorption and re-emission of infrared radiation in the dust layer, the net thermal surface loss is reduced. Therefore a thick dust cloud leads to less reduced temperatures than one of intermediate thickness. This behavior, together with the fact that the lifetime of a dust cloud does not increase with the initial amount of dust or impactor diameter (Figures 2 and 9), explains that at low latitudes the maximum temperature deviations do not increase monotonically with impactor size (Figure 13). We conclude that large impactors (10 km diameter) perturb climate not much longer than 5 km sized bolides.

[66] At high latitudes, in the absence of a dust layer, the annually integrated solar irradiation is roughly half as strong as at the equator. However, owing to meridional atmospheric and ocean transport of thermal energy from the equatorial regions toward the poles, polar and equatorial temperatures are not as different as could be expected from considering solar radiation alone, making the ratio of infrared energy emitted at the equator and in polar regions less than 2 [*Salby*, 1995].

[67] While at the equator, meridional heat transport is a sink, it is a source of energy at middle and high latitudes. This has implications in a situation with an impact induced dust cover. At low latitudes, we observe a drop in temperature, mainly owing to the blocking of sunlight. However,

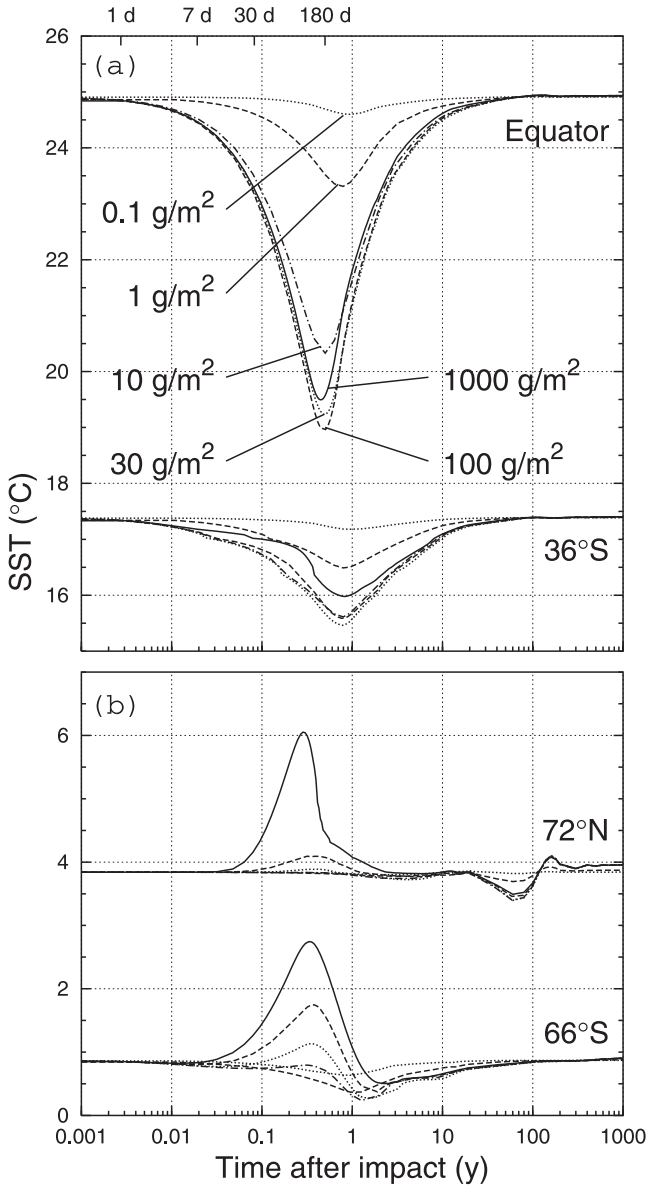

Figure 12. Atlantic sea surface temperatures (SST) at latitudes 0°, 36° S, 66° S, and 72° N as a function of time following impacts. Numbers indicate the initial dust column density (using equation (6): 10^{-4}, 0.001, 0.01, 0.03, 0.1, and 1 kg/m^2 correspond to asteroids 0.5, 1, 2.2, 3, 4.8, and 10.3 km diameter). In polar regions a short-term increase in temperatures is observed, which we relate to the thermal shielding effect of a dust layer against loss of infrared energy. At the equator, the maximal temperature drop is not a monotonic function of initial amount of dust and hence the impactor size. See text for an interpretation.

since with increasing latitude the insolation decreases, this blocking of solar energy becomes less severe in absolute terms. To first order, meridional marine and atmospheric heat transport do not cease. Therefore the temperature drop following an impact is largest at the equator and decreases with latitude and is smallest in polar regions. This, and the fact that the emission of infrared radiation to space is prevented by a dust layer, impact induced dust clouds even increase the temperature (Figure 12b) at high latitudes. However, since following an impact, temperatures are depressed at low latitudes, the meridional heat transport from equatorial to polar regions declines with time, which leads eventually even at high latitudes to decreasing temperatures after 1 year.

[68] The insulation against the loss of thermal radiation also affects air temperatures. At high latitudes, the air temperature increases, with a maximum reached about 2 months after the impact (Figure 14). The amplitude of the increase seems to be a monotonic function of dust induced infrared insulation and hence of the asteroid size. There is evidence that these changes in air temperatures are a direct result of atmospheric radiative forcing, and not induced by heat conduction from the sea surface. This follows from the time lag between the temperature response of air and water, and from the result that the amplitude of air temperatures is larger than of sea surface temperatures (Figures 12 and 14). Even at low latitudes, we observe a short-term increase in air temperature, which, however, is weaker than those in polar regions. This increase is followed by decreasing temperatures, reflecting the thermal coupling to falling water temperatures.

[69] While the surface temperature changes are driven by the radiative forcing, the propagation of temperature deviations into lower layers are caused by local convective mixing, large-scale ocean currents and eddy diffusion. This propagation is slow, as is illustrated in Figure 15, showing equatorial temperature changes as a function of depth half a year and 2 years after the impact. After half a year, major temperature anomalies are restricted to the topmost 200 m

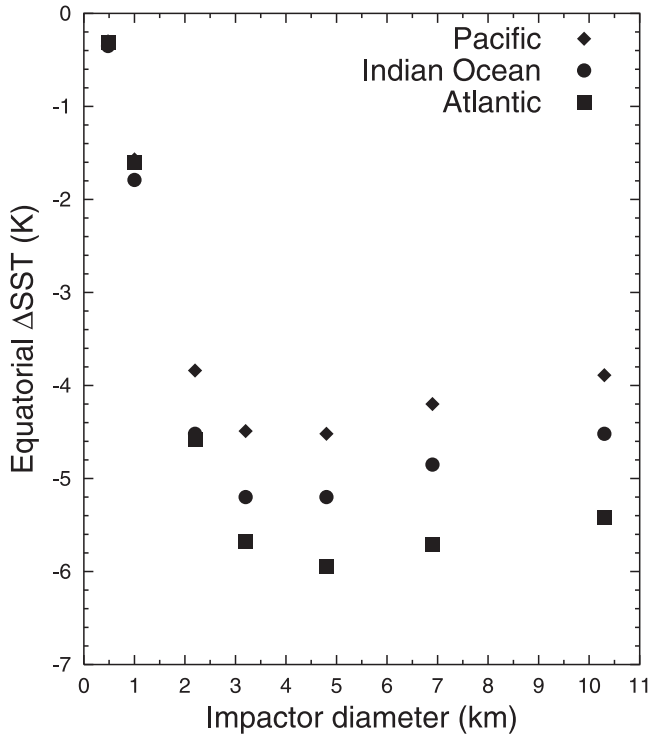

Figure 13. Maximum changes in equatorial sea surface temperatures following impacts as function of impactor size. Asteroid diameters are calculated from initial column densities of the dust clouds by means of expression (6).

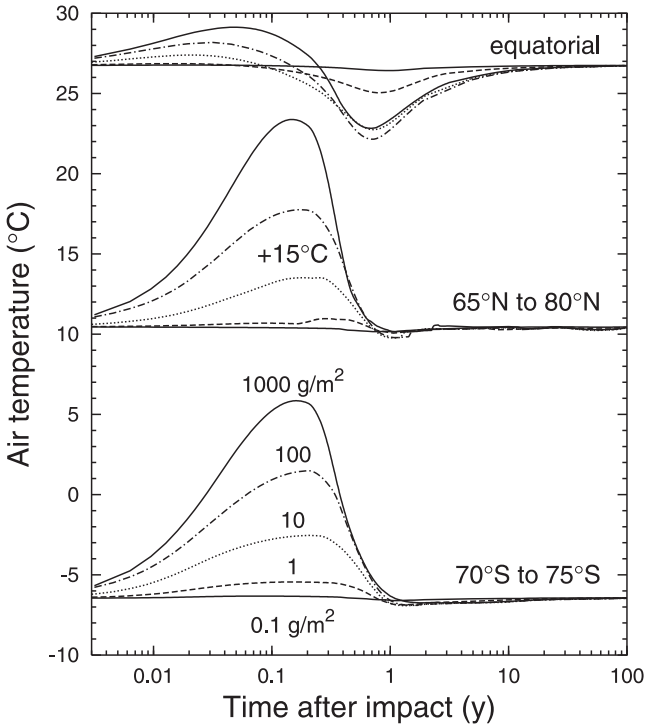

Figure 14. Evolution of air temperatures at low and high latitudes for 5 initial dust column densities (10^{-4}, 0.001, 0.01, 0.1, and 1 kg/m^2). Corresponding sizes of impacting asteroid are given in the caption of Figure 12. Increasing temperature in the first month following the impact are induced by the dust layer insulation against loss of infrared energy. At low latitudes, air temperature drops because of onset of decreasing sea surface temperatures (see Figure 12). Note that the values for the northern latitude band are shifted by + 15°C for clarity of the figure.

of the ocean even for the large impacts. Below the depth of 200 m, the deviations are smaller than 0.1°C. 1.5 years later, deviations at the surface have declined, while in deeper layers, temperature changes have increased.

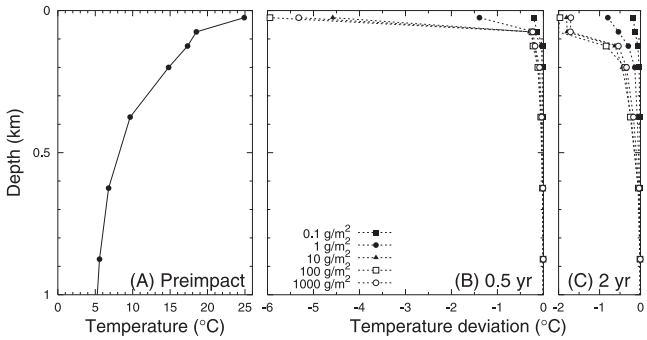

Figure 15. (a) Atlantic temperature profile at equator from the surface to a depth of 1 km before the impact. (b) Profile of temperature deviation 0.5 years after the impact of asteroids leading to initial dust column densities of 10^{-4}, 0.001, 0.01, 0.1, and 1 kg/m^2 (corresponding impactors diameters are given in the caption of Figure 12). (c) Profile of temperature deviation 2 years after the impact.

[70] In simulations of perturbations of the climate system, there is always a potential possibility that the Atlantic meridional overturning circulation, of which the Gulf Stream is one element, may cease. However, we did not observe such an effect as a consequence of impacts. As is illustrated in Figure 16, the strength of the Atlantic meridional overturning circulation shows variability lasting for centuries. The amplitude of these variations is too weak to induce a breakdown of the circulation. In the next section we will show that even a static dust layer with a life time of 2 years does not suffice to destroy the stability of the overturning circulation. However, if the dust layer remained for 5 years, the Atlantic circulation would break down. Interestingly, for impacts of asteroids with diameter larger than 2 km, the strength of the circulation 1 kyr after the impact is not identical to the preimpact level, suggesting that the climate system passes through transient states and finally reaches a new equilibrium slightly different from the state before the impact, although the dust cover has disappeared long ago.

[71] The variations in the meridional overturning can be explained by temporal temperature and salinity variations in the surface of the northern Atlantic. There, under normal conditions, the density of water is relatively high owing to low temperatures and high salinity. Hence the water column is unstable and deep water is formed, which is the important driver for the meridional Atlantic overturning. Deep water formation and overturning is therefore a function of the local mass density at the surface.

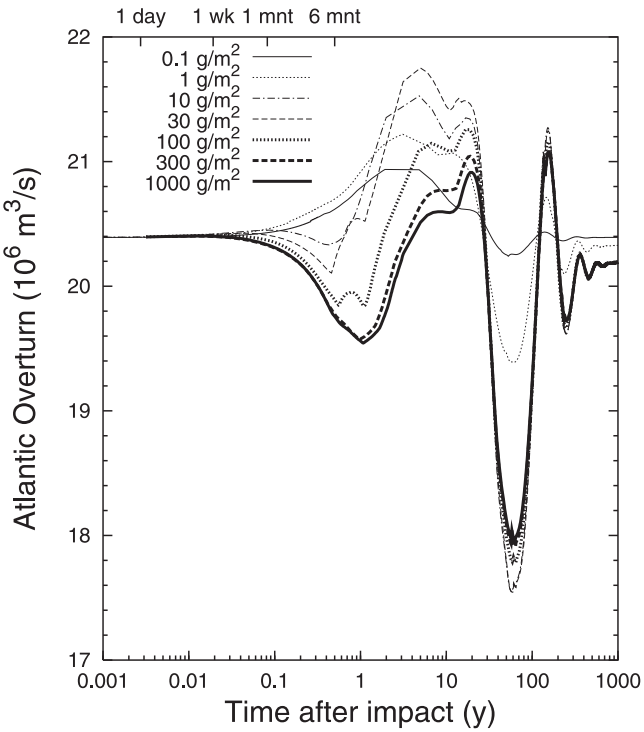

Figure 16. Evolution of maximum meridional overturning circulation of the Atlantic following the impacts of asteroids leading to initial amounts of global dust between 10^{-4} and 1 kg/m^2 (corresponding diameters of impactors are given in the caption for Figure 12).

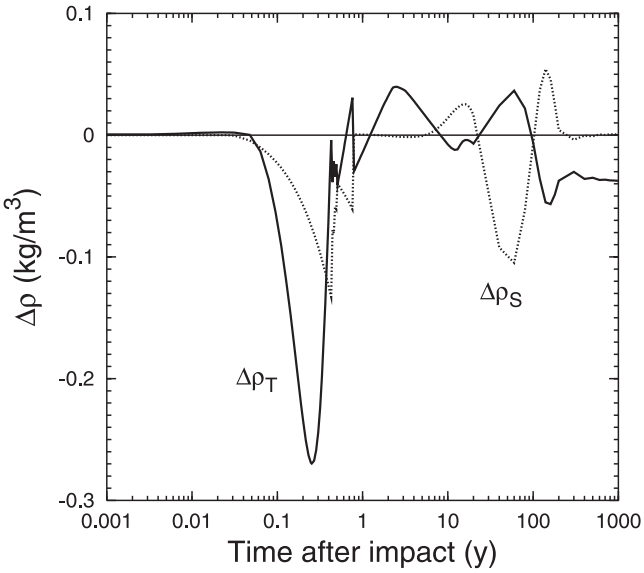

Figure 17. Density variations at the northern Atlantic surface at 60° owing to temperature and salinity deviations ($\Delta\rho_{(T)}$ and $\Delta\ \rho_{(S)}$), which are responsible for the variations in the meridional Atlantic overturning (Figure 16).

[72] For a 10 km sized asteroid impact, the effect of temperature and salinity changes on density variations at the surface of the northern Atlantic is shown in Figure 17. The short-term increase in temperature at high latitudes (Figure 12) decreases the density during the first half year following the impact. During this period, salinity affects the density with the same sign, although with a smaller amplitude. Since a reduction in water density at the surface reduces the instability of the water column, this density decrease is responsible for the reduction of the meridional overturning culminating in the first year (Figure 16). In the period starting 1 year after the impact and ending roughly 10 years later, both temperature and salinity tend to increase density (Figure 17), therefore the Atlantic overturning is enhanced. However, the minimum in the overturning, occurring 60 years after the impact, is only induced by salinity changes, which decrease the density of the northern Atlantic surface water.

6.2. Variation of Refractive Index and Vertical Ocean Eddy Diffusivity

[73] The spectral complex index of refraction used in the radiation transfer module is a material constant of the ejected dust, thus depending on the material at the impact site and the composition of the impactor. Owing to this dependency, we do not expect that the index values we have taken from *Jaenike* [1988], which there have been entitled "dust-like," are a perfect representation of the dust of all possible impacts. Therefore in one case, we have multiplied the imaginary part of the complex refractive index by a factor of 2. The influence of this change on the climatic response is depicted in Figure 18 showing the sea surface (SST) at the equator and at latitude of 36° south. Rather unexpectedly since increasing the imaginary index enhances the optical depth of a medium, the resulting temperature drop is smaller for the case with doubled imaginary part. However, the influence of this doubling is much stronger in the infrared than in the visible, reducing solar input but increasing even more the insulation of terrestrial radiation. Therefore the terrestrial cooling is reduced.

[74] In general, a poorly determined parameter of ocean circulation models is the diffusion coefficient for vertical eddy diffusivity. To determine the importance of this parameter, we performed two model runs using vertical diffusivities of 50% and 200%, respectively, of the nominal value (4×10^{-5} m^2/s). The impact of these changes on the variation of sea surface temperature is marginal (Figure 19).

6.3. Changes in Dust Evolution

6.3.1. One Week Time Lag and 10-Fold Slowed Evolution

[75] The insertion of an artificial one week period, during which the dust distribution remains as it is injected into the atmosphere, has only a slight effect on the climatic change (Figure 20) compared to the reference case. The amplitude of the temperature change is enhanced by about 0.15°C at the equator, which is merely a 3% change in the amplitude. At 36° S the difference to the reference case is even smaller.

[76] A dramatic increase in temperature response is induced if the stratospheric dust evolution is slowed down by a factor of 10 (Figure 20). If the Atlantic temperature drop at the equator is taken as a measure, the amplitude grows by a factor of 2.4. This is far from 10, showing that the climatic response is not simply linear with the amount of dust or dust residence time. However, the magnitude of the Atlantic overturn and the formation of bottom water in the northern Atlantic show substantial variations after the prolonged dust evolution while the variations in the refer-

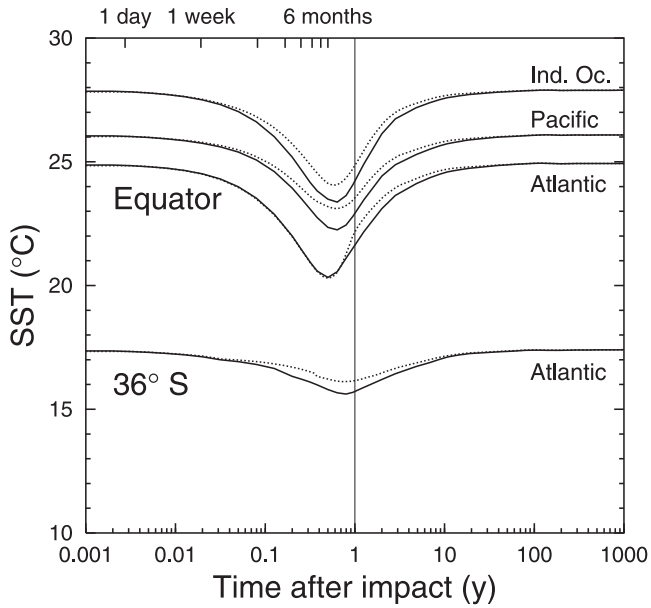

Figure 18. Comparison of doubled imaginary part of refractive index (broken line) with standard case (solid line) using SST at equator (Pacific, Atlantic, and Indian Ocean) and at latitude 36°S (only Atlantic). The initial dust column density is 0.01 kg/m^2. Nominal values of spectral refractive index are shown in Figure 4.

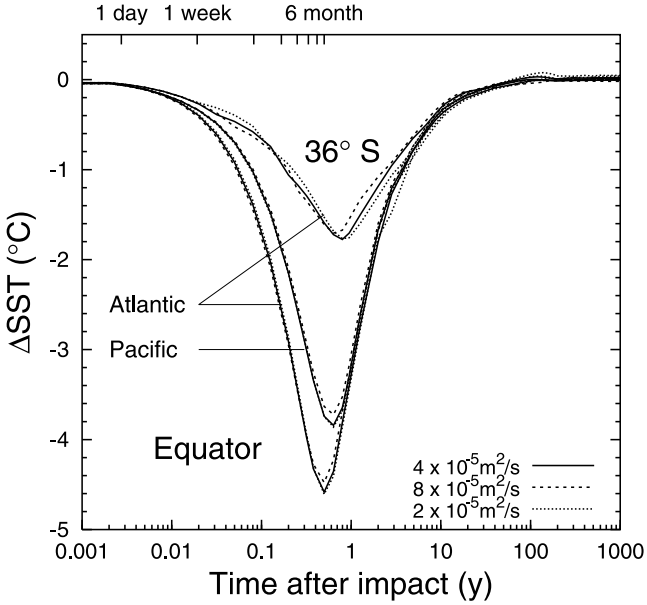

Figure 19. Change of SST at equator (Pacific and Atlantic) and at latitude 36°S (only Atlantic) after an impact for different vertical eddy diffusivities in the ocean model. The nominal value is 4×10^{-5} m^2/s. The initial impact induced dust column density is 0.01 kg/m^2.

ence case are minor (Figure 21). In the first 20 years following the impact, the Atlantic overturn more than doubles in the 10 times prolonged dust cast, then reduces to 25% of the preimpact value, followed by oscillations

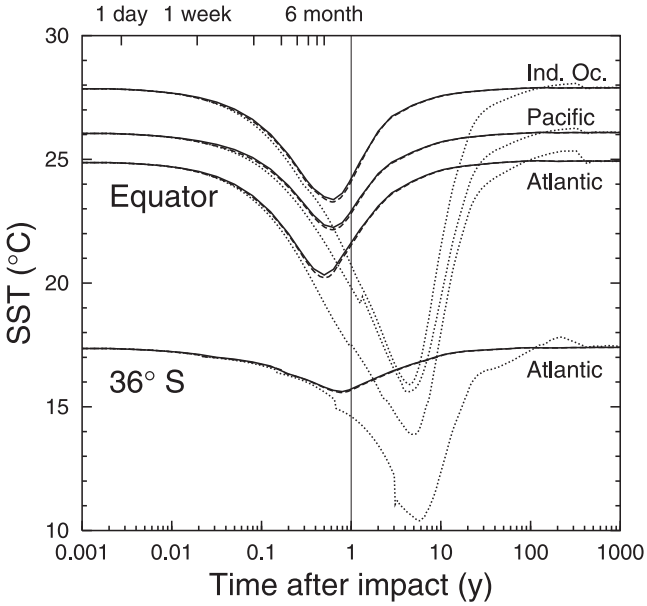

Figure 20. SST at equator (Pacific, Indian Ocean and Atlantic) and latitude 36°S (only Atlantic) after impact (0.01 kg/m^2 initial dust column density). The insertion of a 1 week period immediately after the impact during which the dust evolution is stopped (broken line) shows only a marginal difference compared with the reference case (solid line). However, if the dust evolved 10 times as slowly as in the standard case, then the climatic effects would increase dramatically (dotted line).

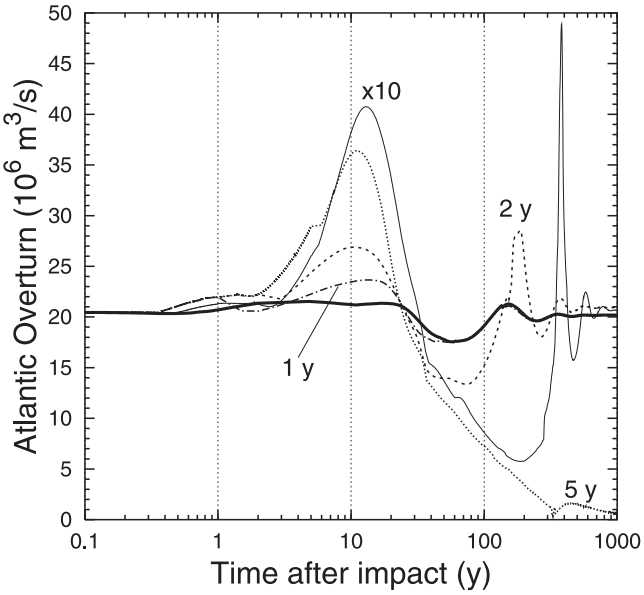

Figure 21. Atlantic overturn circulation after the impact (initial 0.01 kg/m^2 dust column density). In the standard case (heavy solid line), the amplitude of variations are 10% of the preimpact value. "1 y," "2 y," and "5 y" denominate unrealistic cases with static dust layers for 1 year, 2 years, and 5 years following the impact. In the "5 y" case the Atlantic circulation breaks down (dotted line), while in the "2 y" case the changes in overturn are significantly smaller. "x10" is a case where the evolution of the dust in the standard case is slowed down by a factor of 10, showing variations of similar amplitudes like the "5 y" case.

over several 100 years. However, these are probably model intrinsic [*Aeberhardt et al.*, 2000].

6.3.2. Static Dust Layer for 1, 2, and 5 Years

[77] Figure 21 illustrates that in the standard case the climatic perturbation is not strong enough to let the overturn circulation in the Atlantic collapse. To estimate how far the standard case perturbation is from a critical limit, at which the overturn circulation ceases, we greatly enhanced the dust residence time in the atmosphere. To that end, we simulated climate with the artificial assumption that the dust layer remains nonevolving in the atmosphere for a given time (1, 2, and 5 years) after the impact, being instantaneously removed afterward. If the dust lifetime is 1 or 2 years, the variations in the Atlantic Overturning are considerable, but the circulation does not break down (Figure 21). However, the climatic disturbance due to a dust layer remaining static for 5 years leads to a collapse of the overturning after 300 years, which refers to a major climatic change.

[78] Compared to this static dust layer lasting 5 years, the atmospheric residence time of the dust in the standard case is shorter by one order of magnitude (Figure 2, 2.2 km impactor), giving evidence that the standard case is certainly under-critical for a collapse of the Atlantic circulation.

6.3.3. Dust Coagulation

[79] In the nominal cases, coagulation occurs owing to Brownian motion and, at atmospheric levels where the mean free path is longer than the size of dust particles (free molecular regime), owing to gravitational settling (see

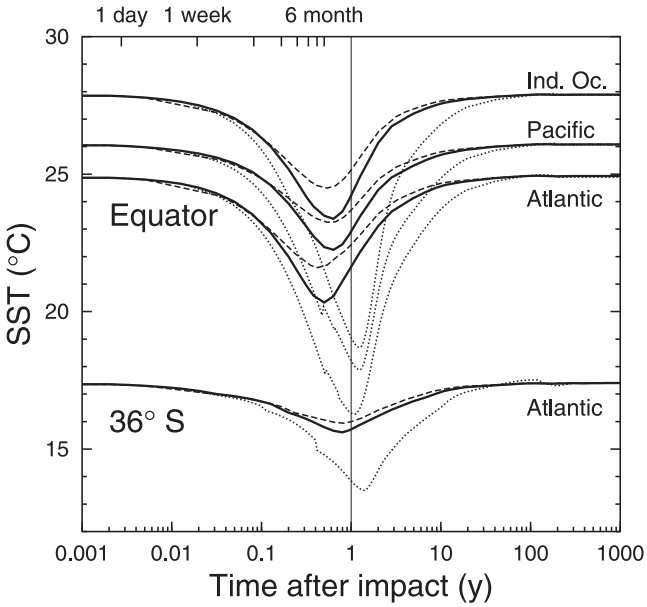

Figure 22. Evolution of SST at equator (Pacific, Indian Ocean, and Atlantic) and latitude 36°S (only Atlantic) after an impact (initial dust column density: 0.01 kg/m^2). Different curves show the effects of variations in the dust evolution module: Coagulation of particles occurs owing to both Brownian motion and gravitational settling (dashed lines), due to both Brownian motion and settling, but restricted to the free molecular flow regime (solid lines, reference case), while dotted lines show the dust evolution when coagulation is not considered. For dust evolution with these model variations, see Figure 2.

section 3.1.2). Beside gravitational settling, coagulation of dust particles is one important mechanism determining the residence time of a dust cloud above the tropopause. If coagulation is not considered at all, significant amounts of dust remain in the atmosphere much longer: a 10-fold reduction of dust column density takes more than 1 year (Figure 2; see also *Toon et al.* [1982]). On the other hand, if coagulation occurs due to settling even in the nonfree molecular regime, the dust column density drops dramatically within a few days.

[80] The influence of these different dust evolution scenarios on climate are presented in Figure 22 showing sea surface temperatures at the equator and at 35°S. Since enhanced coagulation leads to larger particles and hence a shorter lifetime of the dust layer, the temperature deviations in the case with fully included dust coagulation due to settling are smaller than in the standard case. If coagulation is not allowed for, the SST excursions nearly double to 9 K at the equator.

7. Conclusion

[81] We have presented a numerical model to simulate the reactions of climate following impacts of asteroids on the present-day Earth. These impacts contaminate the atmosphere above the tropopause with micron-sized dust particles, which interact with solar and terrestrial radiation. In consequence, present-day radiative energy fluxes are perturbed, and hence the impact may induce climatic changes. To determine the change in the radiation field, we simulated the temporal evolution of impact induced dust clouds including settling and coagulation. Then the transfer of radiation in the visible and the infrared has been calculated. In contrast to previous studies, the oceans and their circulation have been explicitly taken into account, which allows us to follow climatic change over a long period of time.

[82] Since the amount of stratospheric dust is declining after the impact, it is possible to determine a residence time. After a short period of rapid reduction, the decline of the amount of dust is slow, however it does not seem to follow a exponential law as one might suppose. Therefore there is no *e*-fold time to estimate. Instead, we define the residence time as the time after which the amount of stratospheric dust has dropped below a critical value. This threshold is the amount of dust above which radiation energy fluxes are reduced significantly. If the thickness of dust cloud exceeds this limit, the net flux of radiative energy below the dust is significantly disturbed, while lower dust concentrations lead to only slight deviation in radiative fluxes. Using 0.001 kg/m^2 as a critical limit, we find a residence time of climatic relevant amounts of dust between half a year and three quarters of a year, which is in agreement with *Toon et al.* [1982] and *Pollack et al.* [1983].

[83] As follows from the radiation transfer calculations, the optical properties of a given dust cloud may differ vastly in the visible and the infrared. The strong spectral dependency is caused by the fact that the ratio of typical particle size to wavelength is roughly unity for visible wavelengths, but decreases to a fraction of unity in the regime of terrestrial radiation. As shown by the exemplary radiation transfer calculation illustrated, transmission in the visible is smaller than in the infrared by several orders of magnitude, making it difficult for biological processes such as photosynthesis to persist, while significant amounts of solar energy still reach the surface in the near infrared band. In conclusion, we have found surface temperature drops of several degrees at the equator, while with increasing latitude, the temperature deviations decrease. Below the ocean surface, amplitudes of temperature variations decrease drastically with depth. At high latitudes where the solar heating is much smaller than in equatorial regions, the infrared fraction of the total energy flux is dominant. Therefore, in polar regions, the temperature drop is much smaller than at middle and low latitudes. There is even evidence [*Covey et al.*, 1994; *Luder et al.*, 2002] that polar temperatures can increase, which we trace to the infrared insulating effect. Potential uncertainties in refractive index of dust particles do not essentially change these results. An important finding is that the modes of ocean circulation do not change significantly. As an example we note that even for large impacts the Atlantic overturning circulation varies only about 10%. As a set of parameter studies has revealed, much stronger climatic disturbances would be necessary in order to alter the Atlantic overturning. The experiment with a 10-fold decelerated dust evolution, and hence a 10-fold residence time, leads to substantial variations in the circulation, but the Atlantic overturning still recovers to normal. Only a static dust layer suspended for 5 years in the atmosphere has a climatic impact strong enough to cause the circulation to collapse.

[84] Furthermore, temperature drops on Earth's surface are not a monotonically increasing function of the impactor size. Maximal deviations occur for 5 km sized projectiles. However, it would be wrong to deduce that, from a general perspective, 5 km sized impactors are the most threatening ones. Clearly, temperature changes are only one of the many effects of impacts. The magnitude of earthquakes, the extent of ignition of worldwide fires, the production of sulfuric acid, the destruction of the ozone layer do increase in strength with asteroid size well above the 5 km limit.

[85] Because of the wide discrepancy in heat capacity between ocean and land, it was already pointed out in previous studies that the impact induced temperature reactions over the marine surface are much lower than over the continental areas [*Toon et al.*, 1982]. Therefore the variations in continental temperatures reported by *Covey et al.* [1994] are significantly higher than those in sea surface temperature found in this work. Whether the deviations in water temperature of several degrees affect marine life is not straightforward to answer. Diversity of life depends not only on thermal aspects but also on light input and the availability of nutrients, hence it is not possible to relate extinction rates solely to temperature deviations. This does certainly not exclude climate changes following an impact as a potential extinction mechanism, but it seems doubtful that marine temperature drops alone would lead to an extinction event. However, impacts cause a much wider spectrum of consequences [*Toon et al.*, 1997] than only temperature deviation, thus an impact induced extinction event has to be regarded as the result of several contributing effects.

[86] **Acknowledgments.** We are grateful to Andres Hahmann for her helpful review of the manuscript. This work has been supported in part by the Swiss National Science Foundation.

References

Aeberhardt, M., M. Blatter, and T. F. Stocker, Variability on the century time scale and regime changes in a stochastic forced zonally averaged ocean-atmosphere model, *Geophys. Res. Lett.*, *27*, 1303–1306, 2000.

Argyle, E., The global fallout signature of the K/T bolide impact, *Icarus*, *77*, 220–222, 1988.

Berk, A., L. S. Bernstein, and D. C. Robertson, MODTRAN: A moderate resolution model for LOWTRAN 7, *Tech. Rep. GL-TR-89–0122*, 11 pp., Air Force Geophys. Lab., Hanscom AFB, Mass., 1989.

Brown, P., R. E. Spalding, D. O. Revelle, E. Tagliaferri, and S. P. Worden, The flux of small near-Earth objects colliding with Earth, *Nature*, *420*, 294–296, 2002.

Chapman, C. R., and D. Morrison, Impacts on the Earth by asteroids and comets: assessing the hazard, *Nature*, *367*, 33–39, 1994.

Chokshi, A., A. G. G. M. Tielens, and D. Hollenbach, Dust coagulation, *Astrophys. J*, *407*, 806–819, 1993.

Covey, C., S. J. Ghan, and J. J. Walton, Global environmental effects of impact-generated aerosols: Results from a general circulation model, *Spec. Pap. Geol. Soc. Am.*, *247*, 263–270, 1990.

Covey, C., S. L. Thompson, P. R. Weissman, and M. C. MacCracken, Global climatic effects of atmospheric dust from an asteroid or comet impact on Earth, *Global Planet. Change*, *9*, 263–273, 1994.

Crutzen, P. J., and J. W. Birks, The atmosphere after a nuclear war: Twilight at noon, *Ambio*, *11*, 115–125, 1982.

Dominik, C., and A. G. G. M. Tielens, The physics of dust coagulation and the structure of dust aggregates in space, *Astrophys. J.*, *480*, 647–673, 1997.

Durda, D. D., D. A. Kring, E. Pierazzo, and H. J. Melosh, Model calculations of the proximal and globally distributed distal ejecta from the Chicxulub impact crater (abstract), paper presented at 28th Lunar and Planetary Science Conference, Lunar and Planet. Sci. Inst., Houston, Tex., 1997.

Farlow, N. H., V. R. Oberbeck, K. G. Snetsinger, G. V. Ferrey, G. Polkowski, and D. M. Hayes, Size distribution and mineralogy of ash particles in the stratosphere from eruptions of Mount St. Helens, *Science*, *211*, 832–834, 1981.

Goody, R. M., and Y. L. Yung, *Atmospheric Radiation: Theoretical Basis*, 2nd ed., 519 pp., Oxford Univ. Press, New York, 1995.

Grieve, R. A. F., and E. M. Shoemaker, The record of past impacts on Earth, in *Hazards Due to Comets and Asteroids*, edited by T. Gehrels, pp. 417–462, Univ. of Ariz. Press, Tucson, Ariz., 1994.

Hansen, J. E., and L. D. Travis, Light scattering in planetary atmospheres, *Space Sci. Rev.*, *16*, 527–610, 1974.

Hildebrand, A. R., G. T. Penfield, D. A. Kring, M. Pilkington, A. Z. Camargo, S. B. Jacobsen, and W. V. Boynton, Chicxulub impact crater: A possible Cretaceous/Tertiary boundary impact crater on the Yucatan peninsula, Mexico, *Geology*, *19*, 867–871, 1991.

Hills, J. G., I. V. Nemchinov, S. P. Popov, and A. V. Teterev, Tsunami generated by small asteroid impacts, in *Hazards Due to Comets and Asteroids*, edited by T. Gehrels, pp. 779–789, Univ. of Ariz. Press, Tucson, Ariz., 1994.

Irvine, W. M., Multiple scattering in planetary atmospheres, *Icarus*, *25*, 175–204, 1975.

Izett, G. A., G. B. Dalrymple, and L. W. Snee, $^{40}Ar/^{39}Ar$ age of Cretaceous-Tertiary boundary tektites from Haiti, *Science*, *252*, 1539–1542, 1991.

Jaenike, R., Properties of atmospheric aerosols, in *Meteorology: Properties of the Air*, vol. V/4b, edited by G. Fischer, pp. 405–428, Springer-Verlag, New York, 1988.

Kneizys, F. X., E. P. Shettle, L. W. Abreu, J. H. Chetwynd, G. P. Anderson, W. O. Galleryd, J. E. A. Selby, and S. A. Clough, *Users Guide to LOWTRAN 7*, *Rep. AFGL-TR-88–0177*, 137 pp., Air Force Geophys. Lab., Hanscom AFB, Mass., 1988.

Kring, D. A., H. J. Melosh, and D. M. Hunten, Impact-induced perturbations of atmospheric sulfur, *Earth Planet. Sci. Lett.*, *140*, 201–212, 1996.

Lewis, J. S., G. H. Watkins, H. Hartmann, and R. G. Prinn, Chemical consequences of major impact events on Earth, *Spec. Pap. Geol. Soc. Am.*, *190*, 215–221, 1982.

Liou, K. N., and T. Sasamori, On the transfer of solar radiation in aerosol atmospheres, *J. Atmos. Sci.*, *32*, 2166–2177, 1975.

Luder, T., W. Benz, and T. F. Stocker, Modeling long-term climatic effects of impact: First results, *Spec. Pap. Geol. Soc. Am.*, *365*, 717–730, 2002.

Melosh, H. J., *Impact Cratering, A Geological Process, Oxford Monogr. Geol. Geophys.*, vol. 11, 245 pp., Oxford Univ. Press, New York, 1989.

Melosh, H. J., N. M. Schneider, K. J. Zahnle, and D. Latham, Ignition of global wildfires at the Cretaceous/Tertiary boundary, *Nature*, *343*, 251–254, 1990.

Morrison, D., C. R. Chapman, and P. Slovic, The impact hazard, in *Hazards Due to Comets and Asteroids*, edited by T. Gehrels, pp. 59–91, Univ. of Ariz. Press, Tucson, Ariz., 1994.

Neukum, G., and B. A. Ivanov, Crater size distribution and impact probabilities on Earth from lunar, terrestrial-planet, and asteroid cratering data, in *Hazards Due to Comets and Asteroids*, edited by T. Gehrels, pp. 359–416, Univ. of Ariz. Press, Tucson, Ariz., 1994.

Ormö, J., A. P. Rossi, and G. Komatsu, Sirente: A possible small impact crater in Italy, *Meteor. Planet. Sci.*, *36*, suppl. A154, 2001.

Otto, E., H. Fissan, S. H. Park, and K. W. Lee, The log-normal size distribution theory of Brownian aerosol coagulation for the entire particle size range: part II: Analytical solution using Dahneke's coagulation kernel, *J. Aerosol. Sci.*, *30*, 17–34, 1999.

Park, S. H., K. W. Lee, E. Otto, and H. Fissan, The log-normal size distribution theory of Brownian aerosol coagulation for the entire particle size range: part I: Analytical solution using the harmonic mean coagulation kernel, *J. Aerosol. Sci.*, *30*, 3–16, 1999.

Pierazzo, E., D. A. Kring, and H. J. Melosh, Hydrocode simulation of the Chicxulub impact event and the production of climatically active gases, *J. Geophys. Res.*, *103*, 28,607–28,625, 1998.

Pollack, J. B., O. B. Toon, T. P. Ackermann, C. P. McKay, and R. P. Turco, Environmental effects of an impact-generated dust cloud: Implications for the Cretaceous-Tertiary extinctions, *Science*, *219*, 287–289, 1983.

Pope, K. O., A. O. Ocampo, and C. E. Duller, Mexican site for K/T impact crater?, *Nature*, *351*, 105, 1991.

Pope, K. O., K. H. Baines, A. C. Ocampo, and B. A. Ivanov, Impact winter and the Cretaceous/Tertiary extinctions: Results of a Chicxulub asteroid impact model, *Earth Planet. Sci. Lett.*, *128*, 719–725, 1994.

Pope, K. O., K. H. Baines, A. C. Ocampo, and B. A. Ivanov, Energy, volatile production, climatic effects of the Chicxulub Cretaceous/Tertiary impact, *J. Geophys. Res.*, *102*, 21,645–21,664, 1997.

Poppe, T., J. Blum, and T. Henning, Analogous experiments on the stickiness of micron-sized preplanetary dust, *Astrophys. J.*, *533*, 454–471, 2000.

Prinn, R. G., and B. Fegley Jr., Bolide impacts, acid rain, biospheric traumas at the Cretaceous-Tertiary boundary, *Earth Planet. Sci. Lett.*, *83*, 1–15, 1987.

Robock, A., New models confirm nuclear winter, *Bull. At. Sci.*, *45*, 32–35, 1989.

Salby, M. L., *Fundamentals of Atmospheric Physics*, 627 pp., Academic, San Diego, Calif., 1995.

Schneider, S. H., and S. L. Thompson, Simulating the climatic effects of nuclear war, *Nature*, *333*, 221–227, 1988.

Sharpton, V. L., G. B. Dalrymple, L. E. Martin, G. Ryder, B. C. Schuraytz, and J. Urrutia-Fucugauchi, New links between the Chicxulub impact structure and the Cretaceous/Tertiary boundary, *Nature*, *359*, 819–821, 1992.

Sigurdsson, H., S. D'Hondt, and S. Carey, The impact of the Cretaceous/Tertiary bolide on evaporite terrane and generation of major acid aerosol, *Earth Planet. Sci. Lett.*, *109*, 543–559, 1992.

Stamnes, K., The theory of multiple scattering of radiation in plane parallel atmospheres, *Rev. Geophys.*, *24*, 299–310, 1986.

Stocker, T. F., D. G. Wright, and L. A. Mysak, A zonally averaged, coupled ocean-atmosphere model for paleoclimate studies, *J. Clim.*, *5*, 773–797, 1992.

Swisher, C. C., III, et al., Coeval $^{40}Ar/^{39}Ar$ ages of 65.0 million years ago from Chicxulub crater melt rock and Cretaceous-Tertiary boundary tektites, *Science*, *257*, 954–958, 1992.

Thomas, G. E., and K. Stamnes, *Radiative Transfer in the Atmosphere and Ocean*, 517 pp., Cambridge Univ. Press, New York, 1999.

Toon, O. B., J. B. Pollack, T. P. Ackermann, R. P. Turco, C. P. McKay, and M. S. Liu, Evolution of an impact-generated dust cloud and its effects on the atmosphere, *Spec. Pap. Geol. Soc. Am.*, vol. 190, 187–200, 1982.

Toon, O. B., K. Zahnle, D. Morrison, R. P. Turco, and C. Covey, Environmental perturbations caused by the impacts of asteroids and comets, *Rev. Geophys.*, *35*, 41–78, 1997.

Turco, R. P., O. B. Toon, T. P. Ackerman, J. B. Pollack, and C. Sagan, Nuclear winter: Global consequences of multiple nuclear explosions, *Science*, *222*, 1283–1291, 1983.

Turco, R. P., O. B. Toon, T. P. Ackerman, J. B. Pollack, and C. Sagan, Climate and smoke: An appraisal of nuclear war, *Science*, *227*, 166–176, 1990.

Turco, R. P., O. B. Toon, T. P. Ackerman, J. B. Pollack, and C. Sagan, Nuclear winter: Physics and physical mechanisms, *Annu. Rev. Earth Planet. Sci.*, *19*, 383–422, 1991.

Ward, S. N., and E. Asphaug, Asteroid impact tsunami: A probabilistic hazard management, *Icarus*, *145*, 64–78, 2000.

Warneck, P., *Chemistry of the Natural Atmosphere, Int. Geophys. Ser.*, vol. 41, Academic, San Diego, Calif., 1988.

Wolbach, W. S., I. Gilmour, and E. Anders, Major wildfires at the Cretaceous/Tertiary boundary, *Spec. Pap. Geol. Soc. Am.*, *247*, 391–400, 1990.

Wright, D. G., and T. F. Stocker, Sensitivities of a zonally averaged global ocean circulation model, *J. Geophys. Res.*, *97*, 12,707–12,730, 1992.

Zahnle, K. J., Atmospheric chemistry by large impacts, *Spec. Pap. Geol. Soc. Am.*, *247*, 271–288, 1990.

W. Benz, T. Luder, and T. F. Stocker, Physics Institute, Space Research and Planetary Sciences, University of Bern, Sidlerstrasse 5, CH-3012 Bern, Switzerland. (willy.benz@phim.unibe.ch; thomas.luder@phim.unibe.ch; stocker@climate.unibe.ch)